Journal of Computational Chemistry

WILEY

Journal of COMPUTATIONAL CHEMISTRY

RESEARCH ARTICLE

Thermodynamic Stability in Transition Metal-Hydrogen Dications: Potential Energy Curves, Spectroscopic Parameters, and Bonding for VH^{2+}

João Gabriel Farias Romeu[1] | Fernando R. Ornellas[2]

[1]The University of Alabama, Department of Chemistry and Biochemistry, Tuscaloosa, Alabama, USA | [2]Universidade de São Paulo, Instituto de Química, Departamento de Química Fundamental, São Paulo, Brazil

Correspondence: Fernando R. Ornellas (frornell@usp.br)

Received: 10 September 2024 | **Revised:** 24 October 2024 | **Accepted:** 27 October 2024

Funding: This work was supported by Fundação de Amparo à Pesquisa do Estado de São Paulo (FAPESP, Grant # 18/14845-6).

Keywords: bonding | ion-induced dipole interaction | potential energy curves | relativistic states | spectroscopic parameters | thermodynamic stability | transition metal-containing diatomic dications

ABSTRACT

Seventeen electronic states of the dication VH^{2+} were characterized by the SA-CASSCF/icMRCI methodology using very extended basis sets; 11 were described for the first time. Potential energy curves were constructed and the associated spectroscopic parameters evaluated. Triplet and quintet states correlating with the $V^{2+} + H$ channel are thermodynamic stable. For states dissociating into the channel $V^+ + H^+$, avoided crossings at large distances give rise to thermodynamic metastability but do not affect the characterization of the bound region. Configuration state functions with the 3σ orbital /doubly occupied give rise to covalent contributions to the bonding; the major contribution, however, comes from the electrostatic charge-induced dipole interaction. This explains the shape and proximity of the potential energy curves beyond their equilibrium distances. Dipole moment functions and vibrationally averaged dipole moments quantify the polarity of the molecule. Spin–orbit couplings give rise to complex and dense regions of very close-lying Ω states.

1 | Introduction

Theoretical and experimental investigations on doubly charged diatomics, besides their academic interest, have also been extended to areas as diverse as ionosphere chemistry, astrophysical processes, and modeling of gaseous plasmas. We remind that it all started with He_2^{2+} in a study by Pauling back in 1933 [1]. For helium-containing diatomic dications, in particular, studies on the series HeX^{n+} (X = Li–Ne; $n = 1, 2$) by Frenking et al. [2] have shown a rich helium ion chemistry. Besides presenting a comparative analysis of spectroscopic properties for the whole series, they provided a rationale in terms of a relatively simple donor–acceptor model for bonding in this series that can also be extended to other noble gases. More generally, two recent research areas suffice to attest the relevance of diatomic dications studies. First, we note that models of erosion processes of Solar system planets have been reviewed to consider the role these species can play in planetary atmospheric escape and has become a major focus of research by Thissen et al. [3], Lilensten et al. [4], and Falcinelli et al. [5, 6] Second, is the study of gas-phase bimolecular reactions, where the role of electron transfer and bond-formation has been recently and extensively reviewed by Price et al. [7].

Over the years, representative overviews of major contributions of experimental and theoretical investigations on doubly charged dications have been presented by our research group.

A sample of these studies includes: ScS^{2+} [8], CrO^{2+} [9], BaX^{2+} (X = O, H) [10], SrX^{2+} (X = H, O) [11], SrX^{2+} (X = F, Cl, Br, I) [12, 13], OH^{2+} [14], CBr^{2+} [15], TeH^{2+} [16], XBr^{2+} (X = Mg, Ba) [17], SnX^{2+} (X = F, Cl, O) [18], BrO^{2+} and NBr^{2+} [19]. Thermodynamic stability has been the major focus of most of these investigations. Studies involving main group element-containing diatomic dications are relatively abundant in the literature. When diatomic dications containing transition metals are considered, the scarcity of investigations on energetic, structural, and spectroscopic aspects of these systems was first pointed out by Kunze and Harrison in their theoretical work on ScN^{2+} [20]. Thermodynamic stability involving the scandium atom was also reported by Petrie [21] in a thermochemistry study of gas-phase $ScHe^{3+}$ and ScF^{2+}, and by Harrison and Kunze in a series of scandium-nitrogen species of neutral, mono-, and dipositive transition metal nitrides of titanium, vanadium, and chromium [22]. These studies were followed by calculations on transition metal diatomic hydrides by Harrison and Christopher on the series ScH^{2+}, TiH^{2+}, VH^{2+}, CrH^{2+}, and MnH^{2+} [23]. It is also worth noting that systematic investigations of the electronic structure of first-row helides of the type MHe^n, with $n = 0$, +1, +2, and M = Sc−Cu were reported by Wilson et al. [24–26], with further exploration of the isoelectronic analogies between hydrides and helides. Additionally, Klos et al. [27] provided reliable results attesting the thermodynamic stability of $ScHe^{2+}$ and $TiHe^{2+}$.

That the characterization of transition metal-containing diatomics is far from trivial and very challenging, compared with those with only main group atoms [28], is well known in the literature, with this difficulty arising from the closeness of the energy levels of the metal atom that give rise to a high density of relatively low-lying molecular bound states. As extensively demonstrated in our investigations, a further difficulty arises from the fact that the dication dissociation can follow two possible channels, $M^+ + X^+$ and $M^{2+} + X$, and avoided crossings are likely to occur for molecular states with the same spatial and spin symmetries associated with the two channels.

The present work is focused on the VH^{2+} system along the lines of recent investigations on the systems ScS^{2+} [8], and ScH^{2+} [29], mainly focused on their thermodynamic stability. For such, a manifold of triplet and quintet electronic states is characterized by the construction of potential energy curves (PEC), and determination of the most relevant spectroscopic parameters for the states correlating with the lowest dissociation channels; an analysis of the binding process in terms of ion-induced dipole and covalent couplings is presented. Besides the more complete and accurate results here presented, we have also constructed dipole functions and calculated the associated vibrational averages to better quantify the molecular polarity. It is our hope that the reliable results here presented can motivate and guide future experimental investigations on this species and similar systems.

2 | Methodology

The methodological approach used in the investigation of the species VH^{2+} follows essentially the one employed in our previous study of the ScH^{2+} dication. Essentially, the state-averaged complete active space self-consistent (SA-CASSCF) method [30–32] followed by the internally contracted multireference configuration interaction method with Davidson's correction (icMRCI+Q) [33–36], both implemented in the Molpro suite of programs [37], accounted, respectively, for the non-dynamical and dynamical correlation effects in the electronic structure characterization. For the atomic basis functions, the extended sets of quintuple-zeta quality (aug-cc-pV5Z) developed by Balabanov and Peterson [38] for vanadium, and the one reported by Dunning [39] for hydrogen were used.

As an essential step, the number and symmetry of the electronic states to be investigated followed from a direct application of the Wigner–Witmer rules [40]. An overview of the molecular electronic states correlating with the low-lying electronic states of the atomic/ionic fragments arising from the dissociation of the dication VH^{2+} are summarized in Table 1.

For the dication VH^{2+}, we investigated all the quintet states correlating with the five dissociation channels listed in Table 1. For the triplets, the SA-CASSCF calculation included all the states associated with the 10 lowest-lying dissociation channels (not all given in Table 1), but, in the icMRCI+Q step, code restrictions

TABLE 1 | Λ + S electronic states of the dication VH^{2+}, dissociation channels, and energy separation (in cm^{-1}) at the dissociation limit.

States of separated atoms	Multiplicity	Molecular states	Energies exp.[a]
$V^+ (^5D_g) + H^+$	5	Σ^+, Π, Δ	0
$V^+ (^5F_g) + H^+$	5	$\Sigma^-, \Pi, \Delta, \Phi$	2720
$V^{2+} (^4F_g) + H(^2S_g)$	3, 5	$\Sigma^-, \Pi, \Delta, \Phi$	8352
$V^+ (^3F_g) + H^+$	3	$\Sigma^-, \Pi, \Delta, \Phi$	8697
$V^+ (^3P_{2g}) + H^+$	3	Σ^-, Π	11,503
$V^+ (^3H_g) + H^+$	3	$\Sigma^-, \Pi, \Delta, \Phi, \Gamma, H$	12,428
$V^+ (^3F_{2g}) + H^+$	3	$\Sigma^-, \Pi, \Delta, \Phi$	13,353
$V^+ (^5P_g) + H^+$	5	Σ^+, Π	13,440
$V^{2+} (^4P_g) + H(^2S_g)$	3, 5	Σ^-, Π	19,696

[a]Weighted averaged over the multiplets [41].

have forced us to limit the energy calculation only to the states correlating with the five lowest-lying channels. We note, however, that all the states generated in the SA-CASSCF calculations were used as reference states to obtain the icMRCI+Q results. With this choice, we could describe the major bound and repulsive states of both multiplicities.

For such a large number of relatively close-lying states, the choice of the active space and the type of orbitals comprising this space was not easily task. As in our previous study of ScH^{2+}, our search was mainly directed toward sets/orbitals that would mainly allow reliable descriptions of the bound states. In this way, we attempted to reproduce, as close as possible, the energy differences between the various triplet/quintet states at the dissociation limit, since this is the only experimental information on the systems as given in Table S1. For this system, the final choice of active space, (6, 2, 2, 1)/($6A_1$, $2B_1$, $2B_2$, $1A_2$), was similar to that used for ScH^{2+} and includes the orbitals 3s, 3p, 4s, and 3d of vanadium, and the 1s orbital of hydrogen. As usual, C_{2v} point group symmetry, an Abelian subgroup of the $C_{\infty v}$ point group was used in all calculations. With this choice, the A_1 irreducible representation correlates with the Σ^+, $\Delta_{x^2-y^2}$, and Γ states, the B_1 and B_2 with Φ, and with Π^x and Π^y, respectively, and A_2 with Σ^-, Δ_{xy}, and Γ. In this space, 12 electrons were distributed in all possible ways, thus resulting in CASSCF wave functions of dimensions 24,366 ($^5A_1$), 24,540 ($^5B_1/^5B_2$), 24,564 ($^5A_2$), 11,285 ($^5A_1$), 11,330 ($^5B_1/^5B_2$), and 11,430 ($^5A_2$). The dimensions of the icMRCI wavefunctions ranged from about 19×10^6 for the A_1 symmetry, and 24×10^6 for B_1, B_2, and A_2. This choice was based on the best overall agreement between the energy differences at the dissociation limit obtained in this work and the available experimental data as given in Table S1.

Using the functions constructed by numerical interpolation of the calculated energies as a potential in the solution of the radial Schrödinger equation for the nuclear motion, we next obtained the vibrational energies and wavefunctions using the Intensity program [42]. Following standard fitting procedures as described in the literature [40, 43–45], spectroscopic parameters were then obtained from the vibrational energies. The Intensity program was also employed to calculate vibrationally averaged dipole moments.

Concerning the spin–orbit couplings on the PEC, giving rise to the Ω states, they were estimated by first obtaining the spin–orbit matrix elements at the SA-CASSCF level of theory by mixing all triplet and quintet states separately. Then we replaced the diagonal elements by the energies of the Λ+S states calculated by the icMRCI+Q approach. The energies of the Ω states were next obtained by diagonalizing the matrix of the electronic and spin–orbit operators ($H_{el}+H_{SO}$) in the basis formed by the (Λ+S) eigenstates of H_{el} using the one- and two-electron Breit–Pauli operators [46], as also implemented in the Molpro-2010 suite of programs [37]. The molecular orbitals plots were generated using the program IboView [47].

As to scalar relativistic effects, in our previous study of the system ScH^{2+} [29], we indeed investigated its importance in the comparison of calculated and experimental energy values at the dissociation limit using the aug-cc-pV5Z-DK basis set. The differences turned out to be negligible, but the computational time increased very substantially. Due to the similarity between the two systems, the high computational time involved, and the expected negligible differences, we decided not to evaluate the scalar relativist effect on the study of this system. In the case of

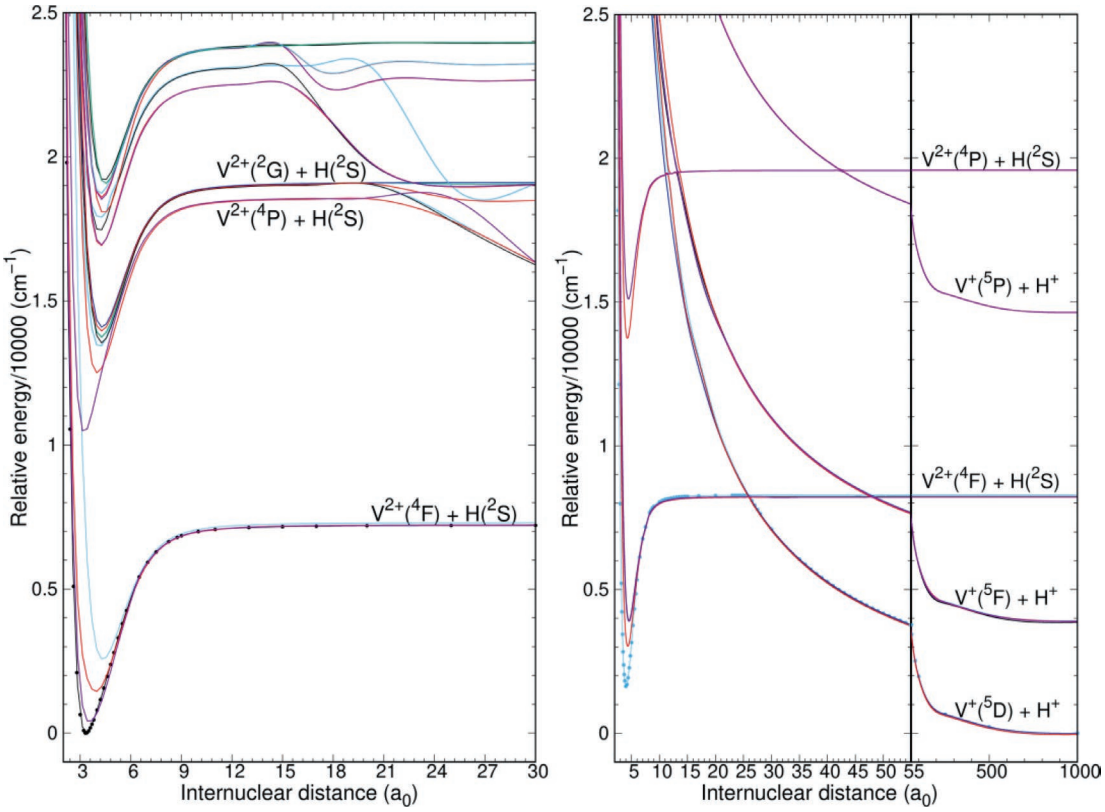

FIGURE 1 | Potential energy curves of the lowest lying Λ+S bound triplet (left) and quintet (right) states of VH^{2+}.

core-correlation effects, we tested its importance in our previous study of the systems VAr^+ and VKr^+ using the aug-cc-pwCV5Z basis sets [48], and similarly, the results turned out to be not significant compared with the valence-only calculations. Since we expected this effect to be much less significant for VH^{2+}, and the considerable increase in computational time involved in the calculation, we also decided not to carry out this calculation in the present study.

3 | Results and Discussion

3.1 | PEC and Spectroscopic Parameters for the Λ + S States

The PEC of the manifold of states investigated are shown in Figure 1 over an extended range of internuclear distances. An expanded and better visualization of the 11-bound triplet and the six-bound quintet states is illustrated in Figure 2, with the corresponding spectroscopic parameters associated with these states and the ones available in the literature collected in Table 2.

As was the case for ScH^{2+}, we can see in Figures 1 and 2 that the more energetic repulsive channels cross the PEC of the bound states at relatively large internuclear distances and are expected to not affect significantly the characterization of the bound states. Keeping this point in mind, we note that the PEC shown for the triplet states are only displayed up to the region of the first crossing with the repulsive states; for the quintets, the description also includes some repulsive states.

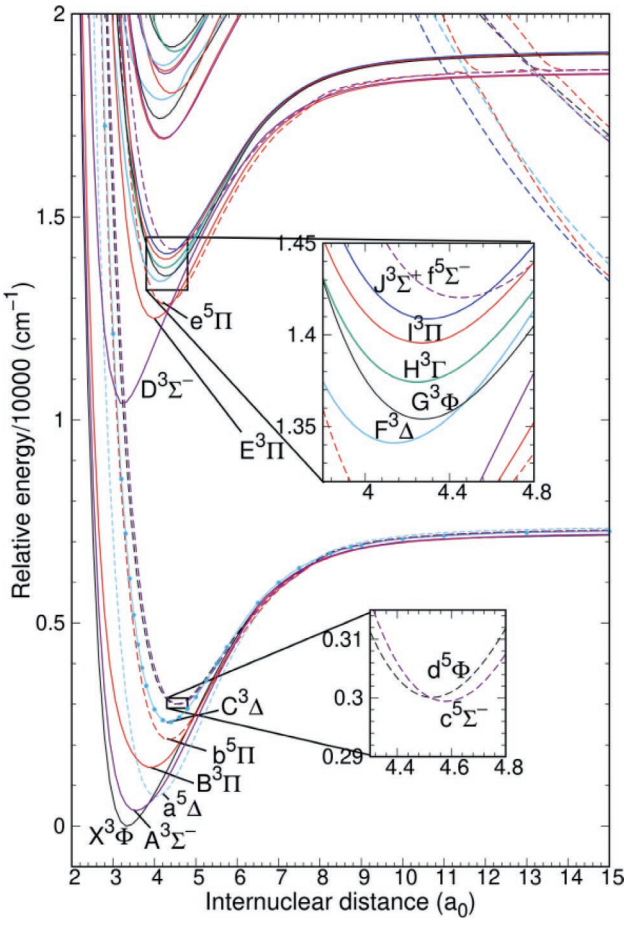

FIGURE 2 | Potential energy curves of the lowest lying Λ+S bound triplet and quintet states of VH^{2+}.

The combined data in Table 1 and Figures 1 and 2 clearly illustrate that for VH^{2+}, since the second ionization potential of the ion V^+ is greater than the ionization potential of the H atom, the two lowest dissociation channels $V^+(5D_g) + H^+$ and $V^+(^5F_g) + H^+$ correlate with repulsive states, with the lowest one giving rise to the states $^5\Sigma^-$, $^5\Pi$, and $^5\Delta$, and the next higher one, at 2720 cm^{-1}, to the states $^5\Sigma^-$, $^5\Pi$, $^5\Delta$, and $^5\Phi$. The next channel, $V^{2+}(^4F_g) + H(^2S_g)$, at 8352 cm^{-1}, correlates with bound states for both triplet and quintet multiplicities. For the triplets, one can clearly see that the four states $^3\Sigma^-$, $^3\Pi$, $^3\Delta$, and $^3\Phi$ are thermodynamic stable. In the case of the quintets, although they are formally metastable, they are expected to be long-lived since the first crossing with a repulsive state occurs at a relatively large distance of about 25 a$_0$ for the lowest channel, and at about 47 a$_0$ for the second one. In this region, charge transfer is very unlikely to occur. As to the higher-lying channel, $V^{2+}(^4P_g) + H(^2S_g)$, at 19,696 cm^{-1}, a series of triplet bound states are also seen in Figure 1 that in fact are metastable, but long-lived, since a crossing occurs at about 25 a$_0$. Due to the necessary approximations used in the location of the other high-lying triplet states, no conclusive statement can be made about their thermodynamic stability. A similar metastability is also observed for the quintet states, but the crossing here occurs at a shorter distance of about 15 a$_0$.

A distinctive feature seen in the PEC of Figure 2, compared with the corresponding ones for ScH^{2+}, is the number of states, which for VH^{2+} is greater and the curves very close-lying. The equilibrium distance (R_e) and the harmonic vibrational constant (ω_e) obtained in this study for the ground state (X $^3\Phi$), 3.330 a$_0$ and 851 cm^{-1}, differ by about 5% and 21%, respectively, from the values of 3.511 a$_0$ and 703 cm^{-1} obtained by Harrison and Christopher[23] using the icMRCI approach, and those of Wilson et al. [24], 3.479 a$_0$ and 706 cm^{-1}, derived from an icMRCI+Q calculation.

For the dissociation energy (D_e), our estimate of 7230 cm^{-1} is greater (~27%) than those obtained by these authors, 5700 cm^{-1} [23], and 6000 cm^{-1} [24], respectively. Before discussing the results for the other states, the differences noted above for the three sets of calculations merit some consideration. The investigation of Harrison and Christopher [23] was focused on the electronic structure of a series of dications of transition metal (Sc, Ti, V, Cr, Mn) monohydrides. Their major goal was to carry out a comparative analysis of the ordering of the electronic states, bond lengths, dissociation energies, and specially the nature of the bonding in this series. The calculation was carried out using the MCSCF/icMRCI approach with the atomic natural orbital set developed by Bauschlicher [49] and Partridge [50] contracted to (7s6p4d3f2g) for vanadium, and the augmented valence quadruple-zeta set of Dunning [51] with the f orbitals removed for H. For a proper comparison, we note first that the basis sets used in this work for the vanadium and hydrogen atoms are significantly more extended (10s9p7d5f4g3h2i) and the full aug-cc-pV5Z sets, respectively. Second, combined with a relatively larger CASSCF space capable of reliably describing, additionally, the bound triplet and quintet states correlating with the higher-lying channel $V^{2+}(^4P) + H(^2S)$ channel, followed by the application of the icMRCI method on the CASSCF reference

TABLE 2 | Spectroscopic parameters of the triplet and quintet Λ+S electronic states of VH^{2+}.

State		R_e/a_0	T_e/cm^{-1}	ω_e[a]$/cm^{-1}$	$\omega_e x_e/cm^{-1}$	$\omega_e y_e/cm^{-1}$	$\omega_e z_e/cm^{-1}$	D_e[b,c]$/cm^{-1}$
X $^3\Phi$	*This study*	3.330	0	851.1 (8)	39.397	2.956	0.1367	7230
	MRCI [23]	3.517	0	703				5700
	icMRCI [24]	3.479	0	706				6000
A $^3\Sigma^-$	*This study*	3.548	353	726.3 (6)	13.602	0.487	0.0695	6889
	MRCI [23]	3.786	240	643				5600
a $^5\Delta$	*This study*	4.042	703	828.6 (7)	25.089	0.147	0.0254	6662 (−1616)
	MRCI [23]	4.104	81	807				5600
B $^5\Pi$	*This study*	3.918	1430	621.4 (6)	8.524	0.367	0.0729	5817
	MRCI [23]	4.098	970	661				4800
b $^5\Pi$	*This study*	4.354	2117	730.4 (6)	27.211	0.2463	0.0251	5176 (−3075)
	MRCI [23]	4.426	1500	705				4300
C $^3\Delta$	*This study*	4.350	2548	702.1 (5)	28.431	1.503	0.1365	4748
	MRCI [23]	4.428	1800	688				4000
c $^5\Sigma^-$	*This study*	4.583	2988	665.7 (5)	29.568	0.5401	0.0269	4324 (−9)
	MRCI [23]	4.661	2300	655				3500
d $^5\Phi$	*This study*	4.531	2995	673.1 (6)	35.962	2.581	−0.1733	4321 (−52)
	MRCI [23]	4.620	2300	651				3500
D $^3\Sigma^-$	*This study*	3.253	10,418	1078.4 (7)	81.037	7.690	0.3303	8149 (*−2850*)
E $^3\Pi$	*This study*	3.956	12,502	790.9	25.064	0.3654	0.0395	6038 (*−4961*)
e $^5\Pi$	*This study*	4.268	12,828	782.7 (6)	27.110	0.1565	0.0206	5680 (−9849)
F $^3\Delta$	*This study*	4.137	13,406	747.3 (6)	23.509	0.0433	0.0114	5.639 (*−5360*)
G $^3\Phi$	*This study*	4.271	13,512	781.6 (6)	43.661	4.891	0.3179	5545 (*−5454*)
H $^3\Gamma$	*This study*	4.239	13,737	720.3 (6)	24.748	1.674	0.1498	5355 (*−1914*)
I $^3\Pi$	*This study*	4.276	13,958	687.7 (6)	21.267	2.154	0.2319	5074 (*−3120*)
J $^3\Sigma^+$	*This study*	4.272	14,050	714.6 (6)	37.536	4.692	0.3441	5057 (*−2212*)
f $^5\Sigma^-$	*This study*	4.453	14,194	684.7 (5)	32.617	0.9950	0.0433	4394 (−6876)

[a]Figures in parenthesis give the number of points used in the fitting procedure.
[b]Figures in parenthesis refer to the dissociation energy for the repulsive states.
[c]Figures in italics refer to energy estimates based on the experimental energies of the repulsive channels.

spaces, a substantial amount of the dynamic correlation energy is recovered, thus guaranteeing a more accurate description of the PEC and the associated spectroscopic parameters in this work. Harrison and Christopher calculation was restricted to the covalent channel only. As to the investigation of Wilson et al. [24], it focused mainly on the spectroscopic parameters of the ground state using the SA-MCSCF/icMRCI+Q approach for the construction of the PEC. The basis sets employed are significantly smaller, (8 s, 7p, 5d, 2f, 1 g) for vanadium, and the aug-cc-pVQZ for hydrogen. Also, their active space, by including only the 3d and 4s orbitals of the vanadium atom, and the 1s of hydrogen was much smaller, thus making the recovering of both non-dynamic and dynamic correlation effects less effective than in the present study; the agreement between these two studies for the reported values for R_e, D_e, and ω_e is expected since their levels of calculation are very similar.

Another important point accounting for the differences in the harmonic vibrational frequencies is the absence of anharmonic vibrational constants in the reported results of these authors. It is well known that the determination of spectroscopic parameters either experimental or theoretical is dependent on the number of adjustable parameters and the number of fitting data as discussed by Richards et al. [52] The two studies do not take into account the contributions of anharmonicities in the potential on the evaluation of the spectroscopic parameters constants and the consequence is evident in Table 2.

A comparison of the ground state spectroscopic parameters of VH^{2+} with those of ScH^{2+} is instructive in showing that the bonding in VH^{2+} is weaker than that in ScH^{2+}: R_e/a_0 (3.201; 3.330), ω_e/cm^{-1} (1603; 851), $\omega_e x_e/cm^{-1}$ (63.7; 39.4), and D_e/cm^{-1} (12,731; 7230); in this sequence, the first numerical entry refers

to ScH^{2+} and the second one to VH^{2+}. For the other excited states associated with the first dissociation channel, we noted a similar behavior as the one obtained for ScH^{2+}, namely, a shortening of R_e ranging between 0.1 and 0.3 a_0; an increase in the excitation energies (T_e), and a decrease in the dissociation energies by about 1000 cm^{-1}, all relative to the results of Harrison and Christopher [23].

In the case of the vibrational constants, our values are greater by 1%–13%. We note again that the reported values in the literature do not take into account the anharmonicities of the PEC. In our study, the inclusion in the fitting equation of the parameter $\omega_e z_e$ was also necessary for more consistent results. A final difference in the order of the states A [3]Σ^- and a $^5\Delta$ should also be noted in the work of Harrison and Christopher. For all the other excited states associated with the second and third dissociation channels, this is their first characterization in the literature; they are predicted to be metastable. In Table 2, due to a code impossibility of including all the triplet states listed in Table 1 in the CASSCF/MRCI procedure, the dissociation energies associated with the repulsive states were estimated using also the available experimental energies; this was not the case for the quintet states, where the energy differences were derived from the calculated values. Thermodynamically, the state e $^5\Pi$ was estimated as the least stable, whereas the state D $^3\Sigma^-$showed the largest dissociation barrier for a bound state and the largest harmonic vibrational constant. Vibrational energy spacings, $\Delta G_{v+1/2}$, and zero-point energies for all bound states are collected in Tables S2 and S3 for the electronic states of the dication VH^{2+}; and additionally, the rotational constants B_v, B_e, and α_e are given in Tables S4 and S5, all as Supporting Information S1.

The major contributions of the configuration state functions characterizing the states investigated are collected in Table 3, and in Figure 3 the spatial distributions of representative orbitals of VH^{2+} in the ground state are illustrated for the internuclear distance of 3.2 a_0. Note that the ground state X $^3\Phi$ can be represented by the mixture of determinants 0.547 ($|1\sigma^2\ 2\sigma^2\ 3\sigma^2 1\delta^1 1\pi^4 2\pi_y^{\ 1}\rangle + |1\sigma^2\ 2\sigma^2\ 3\sigma^2 1\delta^1 1\pi^4 2\pi_x^{\ 1}\rangle$), where the orbitals 1σ, 2σ, and 1π are mainly localized on the vanadium moiety; as to the orbital 3σ, it clearly displays an overlap between the vanadium δ_σ orbital with the hydrogen 1 s, a reflection of a covalent bond contribution to the stability of this state, similarly as observed for ScH^{2+}, as shown in Figure 3. In the case of the orbitals 1δ and 2π, there are clearly V-localized. It is interesting to note in Figure 3 that all bound states correlating with the covalent channel, by having very close-lying PEC beyond their equilibrium distances, they also reflect the important contribution of the ion-induced dipole interaction for the stability of these states. In fact, taking $-0.5\alpha \times q^2/R^4$ (in a.u.) for this interaction energy, where a is the polarizability of the hydrogen atom (9/2 a_0^3 in a.u.), q the vanadium ion charge, and R the internuclear distance, this contribution amounts to −0.0144 a.u. (~3150 cm^{-1}) for $R = 5.0$ a_0, a result easily verified in Figure 3. The double occupancy of orbital 3σ, essentially a d_0(V)–s(H) mixture, also accounts for the covalent contribution in the excited states, besides the electrostatic one; states with single occupancy of 3σ in the reference function show a decrease in the estimated bond energy, as given in Table 2. Also evident in Figure 2 and Table 2 is the metastability of most bound excited states, a result of the avoided crossings of the repulsive curves with the ones arising from the ion-induced dipole contribution; covalent also plays a role for these states, as one can verify from the 3σ occupancy.

TABLE 3 | Major contributions of the configuration state functions at the equilibrium distance of VH^{2+}.

State	Configurations
X $^3\Phi$	$0.547\ (\|1\sigma^2\ 2\sigma^2\ 3\sigma^2 1\delta^1 1\pi^4 2\pi_y^{\ 1}\rangle + \|1\sigma^2\ 2\sigma^2\ 3\sigma^2 1\delta^1 1\pi^4 2\pi_x^{\ 1}\rangle)$
A $^3\Sigma^-$	$0.654\ \|1\sigma^2\ 2\sigma^2\ 3\sigma^2 1\delta^2 1\pi^4\rangle + 0.399\ \|1\sigma^2\ 2\sigma^2\ 3\sigma^1\ 4\sigma^1 1\delta^2 1\pi^4\rangle + 0.390\ \|1\sigma^2\ 2\sigma^2\ 3\sigma^2 1\pi^4 2\pi^2\rangle$
B $^3\Pi$	$0.505\ (\|1\sigma^2\ 2\sigma^2\ 3\sigma^2 1\delta^1 1\pi^4 2\pi_y^{\ 1}\rangle + \|1\sigma^2\ 2\sigma^2\ 3\sigma^2 1\delta^1 1\pi^4 2\pi_x^{\ 1}\rangle)$
C $^3\Delta$	$0.829\ \|1\sigma^2\ 2\sigma^2\ 3\sigma^\alpha 1\delta^\alpha 1\pi^4 2\pi^2\rangle + 0.418\ \|1\sigma^2\ 2\sigma^2\ 3\sigma^\alpha 1\delta^\beta 1\pi^4\ 2\pi_x^{\ \alpha} 2\pi_x^{\ \alpha}\rangle$
D $^3\Sigma^-$	$0.698\ \|1\sigma^2\ 2\sigma^2\ 3\sigma^2 1\pi^4 2\pi^2\rangle - 0.424\ \|1\sigma^2\ 2\sigma^2\ 3\sigma^1\ 4\sigma^1 1\pi^4 2\pi^2\rangle + 0.358\ \|1\sigma^2\ 2\sigma^2\ 3\sigma^2 1\delta^2 1\pi^4\rangle$
E $^3\Pi$	$0.695\ \|1\sigma^2\ 2\sigma^2\ 3\sigma^1 1\delta^2 1\pi^4 2\pi_x^{\ 1}\rangle + 0.402\ \|1\sigma^2\ 2\sigma^2\ 3\sigma^1 1\delta^2 1\pi^4 2\pi_x^{\ 1}\rangle$
F $^3\Delta$	$0.687\ \|1\sigma^2\ 2\sigma^2\ 3\sigma^2\ 4\sigma^1 1\delta^1 1\pi^4\rangle + 0.464\|\ 1\sigma^2\ 2\sigma^2\ 3\sigma^1\ 4\sigma^2 1\delta^1 1\pi^4\rangle$
G $^3\Phi$	$0.570\ \|1\sigma^2\ 2\sigma^2\ 3\sigma^1 1\pi^4 2\pi^3\rangle - 0.432\ (\|1\sigma^2\ 2\sigma^2\ 3\sigma^1 1\delta^2 1\pi^4 2\pi_y^{\ 1}\rangle + \|1\sigma^2\ 2\sigma^2\ 3\sigma^1 1\delta^2 1\pi^4 2\pi_y^{\ 1}\rangle)$
H $^3\Gamma$	$0.564\ \|1\sigma^2\ 2\sigma^2\ 3\sigma^1 1\delta^1 1\pi^4 2\pi^2\rangle - 0.423\ \|1\sigma^2\ 2\sigma^2\ 3\sigma^1 1\delta^1 1\pi^4 2\pi^2\rangle$
I $^3\Pi$	$0.431\ \|1\sigma^2\ 2\sigma^2\ 3\sigma^1\ 4\sigma^1 1\delta^1 1\pi^4 2\pi_y^{\ 1}\rangle + 0.400\|1\sigma^2\ 2\sigma^2\ 3\sigma^1\ 4\sigma^1 1\delta^1 1\pi^4 2\pi_x^{\ 1}\rangle + 0.393\|1\sigma^2\ 2\sigma^2\ 3\sigma^1\ 4\sigma^1 1\delta^1 1\pi^4 2\pi_x^{\ 1}\rangle$
J $^3\Sigma^+$	$0.574\ \|1\sigma^2\ 2\sigma^2\ 3\sigma^1 1\delta^1 1\pi^4 2\pi^2\rangle + 0.469\ (0.564\ \|1\sigma^2\ 2\sigma^2\ 3\sigma^1 1\delta^1 1\pi^4 2\pi^2\rangle - \|1\sigma^2\ 2\sigma^2\ 3\sigma^1 1\delta^1 1\pi^4 2\pi^2\rangle)$
a $^5\Delta$	$0.979\ \|1\sigma^2\ 2\sigma^2\ 3\sigma^1 1\delta^1 1\pi^4 2\pi^2\rangle - 0.144\ \|1\sigma^2\ 2\sigma^2\ 4\sigma^1 1\delta^1 1\pi^4 2\pi^2\rangle$
b $^5\Pi$	$0.781\ \|1\sigma^2\ 2\sigma^2\ 3\sigma^1 1\delta^2 1\pi^4 2\pi_y^{\ 1}\rangle + 0.375\ (\|1\sigma^2\ 2\sigma^2 3\sigma^1 4\sigma^1 1\delta^1 1\pi^4 2\pi_y^{\ 1}\rangle + \|1\sigma^2\ 2\sigma^2\ 3\sigma^1\ 4\sigma^1\ 1\delta^1 1\pi^4 2\pi_x^{\ 1}\rangle)$
c $^5\Sigma^-$	$0.730\|1\sigma^2\ 2\sigma^2\ 3\sigma^1\ 4\sigma^1 1\delta^2 1\pi^4\rangle + 0.504\|1\sigma^2\ 2\sigma^2\ 3\sigma^1\ 4\sigma^1 1\pi^4 2\pi^2\rangle - 0.379\|1\sigma^2\ 2\sigma^2\ 3\sigma^1\ 5\sigma^1 1\delta^2 1\pi^4\rangle$
d $^5\Phi$	$0.630\ (\|1\sigma^2\ 2\sigma^2 3\sigma^1 4\sigma^1 1\delta^1 1\pi^4 2\pi_y^{\ 1}\rangle - \|1\sigma^2\ 2\sigma^2\ 3\sigma^1\ 4\sigma^1\ 1\delta^1 1\pi^4 2\pi_x^{\ 1}\rangle) + 0.306\ (\|1\sigma^2\ 2\sigma^2 3\sigma^1 5\sigma^1\ 1\delta^1 1\pi^4 2\pi_y^{\ 1}\rangle - \|1\sigma^2\ 2\sigma^2\ 3\sigma^1 5\sigma^1 1\delta^1 1\pi^4 2\pi_x^{\ 1}\rangle)$
e $^5\Pi$	$0.593\ \|1\sigma^2\ 2\sigma^2\ 3\sigma^1 1\delta^2 1\pi^4 2\pi_y^{\ 1}\rangle + 0.508\ (\|1\sigma^2\ 2\sigma^2 3\sigma^1 4\sigma^1 1\delta^1 1\pi^4 2\pi_y^{\ 1}\rangle + \|1\sigma^2\ 2\sigma^2\ 3\sigma^1\ 4\sigma^1\ 1\delta^1 1\pi^4 2\pi_x^{\ 1}\rangle)$
f $^5\Sigma^-$	$0.754\ \|1\sigma^2\ 2\sigma^2\ 3\sigma^1\ 4\sigma^1 1\pi^4 2\pi^2\rangle - 0.486\ \|1\sigma^2\ 2\sigma^2\ 3\sigma^1\ 4\sigma^1 1\delta^2 1\pi^4\rangle + 0.263\ \|1\sigma^2\ 2\sigma^2\ 3\sigma^1\ 5\sigma^1 1\delta^2 1\pi^4\rangle$

As to symmetry of the occupied δ orbital of the ground state, a simple direct application of group theory can help us identify its symmetry. As explicit in the text, the calculation was carried out using the C_{2v} point group symmetry. The energy for the ground state ($^3\Phi$) was obtained by working in the B_1 irreducible representation, so the product of the two orbitals

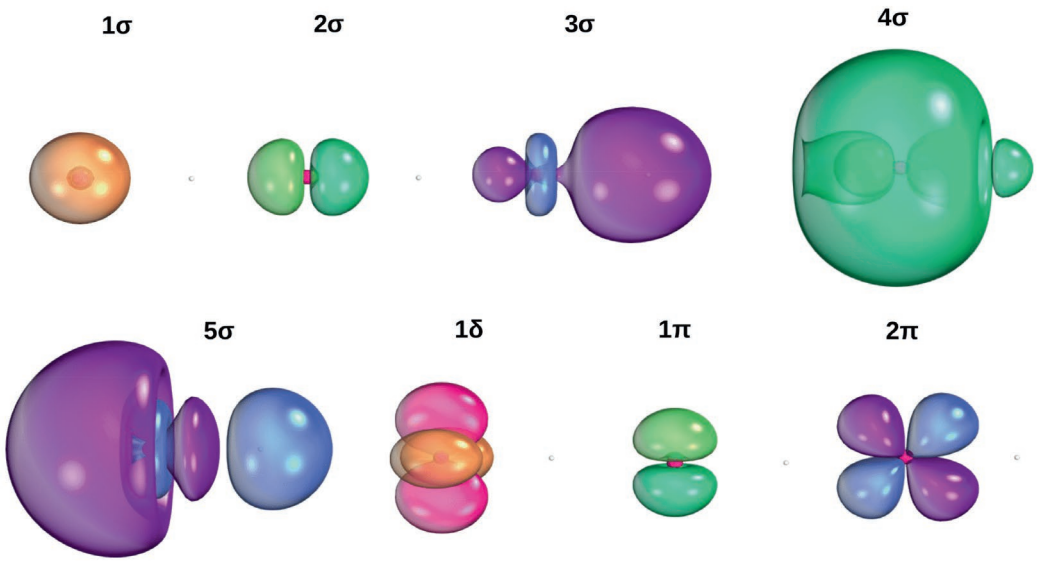

FIGURE 3 | Spatial distribution of major orbitals of the ground state for VH^{2+} at 3.2 a_0. Orbitals composition: $1\sigma \sim 1.0s(V)$; $2\sigma \sim 0.995\ p_z(V)$; $3\sigma \sim 0.274s(V) + 0.342\ d_0(V) - 0.117\ p_z(V) + 1.0s(H)$; $4\sigma \sim 0.596\,s(V)—0.710\ d_0(V) + 0.148\ p_z\ (V) + 0.183s(H)$; $5\sigma \sim 0.465s(V) - 0.195s'(V) + 0.364\,s''(V) + 0.565\ d_0(V) - 0.426\,s(H)$; $1\delta(a_1) \sim 0.988\ d_x2-_y2\ (V)$; $1\delta(a_2) \sim 0.988\ d_{xy}\ (V)$; $1\pi_{x,y} \sim 0.999\ p_{x,y}\ (V)$; $2\pi_{x,y} \sim 0.979\ d_{+/-}$.

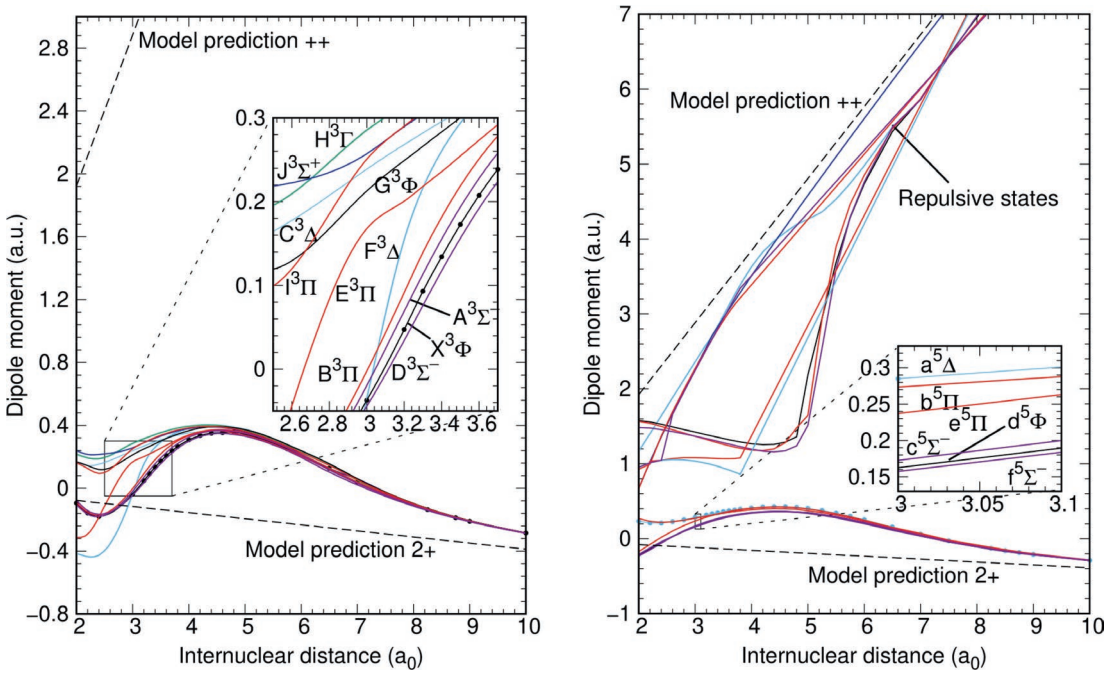

FIGURE 4 | Dipole moment (in a.u.) relative to the center of mass versus the internuclear distance for the triplet (left) and quintet (right) electronic states of VH^{2+}. The dashed line describes the dipole moment of a bare 2+ charge on the metal atom relative to the center of mass. Conversion factor: 1 a.u. = 2.542 Debye.

occupied orbitals should transform according to B_1. For the first determinant, associated with the ground state, we have the product $\delta \times \pi_y$, which corresponds to the product $a_2 \times b_2$, that transforms like B_1, in the C_{2v} notation. So, the first δ orbital should be d_{xy}. As to the second determinant, one has the product $\delta \times \pi_x$ ($a_1 \times b_1$) that also transforms like B_1, leading to the identification of a_1 with the orbital d_{x2-y2}. Similarly, by the direct application of this rule one can identify all the symmetry of all orbitals.

3.2 | Dipole Moment Functions

Complementing this spectroscopic characterization, we show in Figure 4 dipole moment functions relative to the center of mass (default in Molpro) for selected triplet and quintet states. It is not surprising that these functions show a very similar behavior, a reflection of the electronic densities associated with the corresponding PEC. Since the center of mass is very near the vanadium moiety, the magnitudes of the moments are necessarily

TABLE 4 | Relativistic states (Ω) arising from the Λ + S electronic states of VH^{2+}.

Λ + S states	Ω states	Λ + S states	Ω states
X $^3\Phi$	4, 3, 2	E $^3\Pi$	0^-, 0^+, 1, 2
A $^3\Sigma^-$	0^+, 1	e $^5\Pi$	3, 2, 1 (2), 0^+, 0^-
a $^5\Delta$	4, 3, 2, 1, 0^+, 0^-	F $^3\Delta$	3, 2, 1
B $^3\Pi$	0^-, 0^+, 1, 2	G $^3\Phi$	4, 3, 2
b $^5\Pi$	3, 2, 1 (2), 0^+, 0^-	H $^3\Gamma$	5, 4, 3
C $^3\Delta$	3, 2, 1	I $^3\Pi$	0^-, 0^+, 1, 2
c $^5\Sigma^-$	0^-, 1, 2	J $^3\Sigma^+$	0^-, 1
d $^5\Phi$	5, 4, 3, 2, 1	f $^5\Sigma^-$	0^-, 1, 2
D $^3\Sigma^-$	0^-, 1		

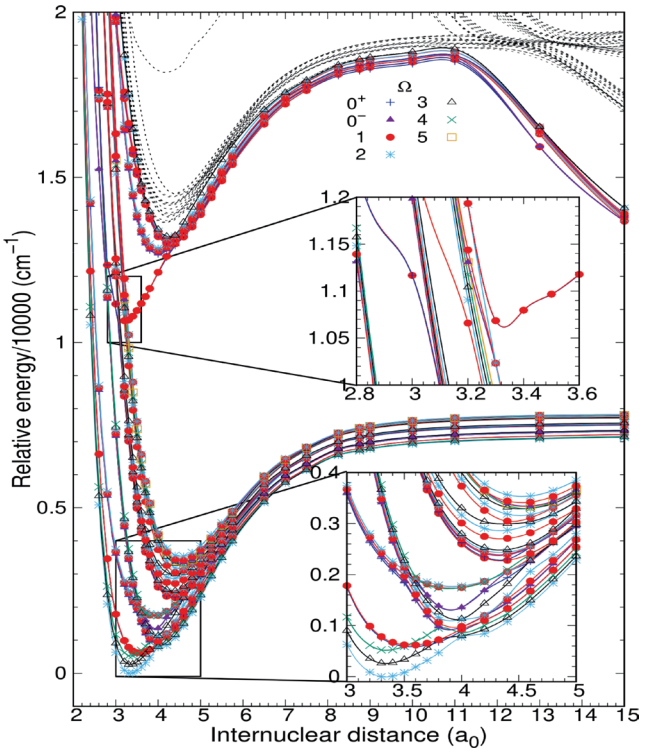

FIGURE 5 | Potential energy curves of the lowest lying Ω states of VH^{2+}.

small. Considering a simplified model with two positive charges located on the vanadium moiety, the dipole moment function is expected to vary as $-0.0388 \times R$, whereas if we place one positive charge on each center, the expected behavior should go as $0.9612 \times R$; these predictions are shown as dashed lines in Figure 3. For long distances, these models agree with the calculated ab initio results. For shorter distances, a shielding effect of the inner electrons of vanadium is responsible for the small changes observed for the different states. For the ground vibrational states ($v = 0$), the polarity of VH^{2+}, in terms of vibrationally averaged dipole moments, followed the order: D < X < A < B < E < f ≈ C ≈ d ≈ c < G ≈ J ≈ F ≈ I < b ≈ H < a ≈ e, with a difference of 0.90 D between the most polar (1.06 D) and the least polar (0.22 D). In Tables S6 and S7, we collected vibrationally averaged dipole moments for the bound states here investigated.

3.3 | The Effect of Spin–Orbit Coupling on the Λ + S States

The effect of spin–orbit couplings on the Λ + S PEC of VH^{2+} is first given in Table 4, where one can see the number of Ω states resulting from the coupling for each non-relativistic state. In Figure 5 we illustrate a manifold of PEC for these states with the inset depicting the curves in the equilibrium region. Due to the very large number of Ω states, the spin–orbit calculation was restricted to the first three dissociation channels associated with the bound states. Overall, as shown in Figure 5, an increase in the density of states is evident, and the changes in these curves are very small, and practically indistinguishable. Despite this closeness, we could identify various avoided crossings for the Ω states arising from the states X $^3\Phi$, A $^3\Sigma^-$, a $^5\Delta$, and B $^3\Pi$. The most significant change occurred for the state D $^3\Sigma^-$ for which the split states D $^3\Sigma_0^-$ and D $^3\Sigma_1^-$ avoid crossings with the states b $^5\Pi_0^+$, b $^5\Pi_1$, C $^3\Delta_1$, c $^5\Sigma_1^-$, and d $^5\Phi_1$. Small changes in the spectroscopic parameters derived for the corresponding Λ + S states are thus expected, but overall the parameters obtained for the other Λ + S states should reliably characterize this system.

4 | Conclusions

A manifold of 17 Λ + S electronic—11 triplets and six quintets—correlating with the lowest dissociation channels of the transition metal-hydride diatomic dication VH^{2+} was investigated at a high level of theory. Nine of these states are described for the first time in the literature. The use of very extended basis sets along with large active spaces, accounting for non-dynamical correlation effects, followed by the incorporation of a substantial amount of dynamical correlation by single and double electron excitations on top of the reference spaces, guarantees a more accurate characterization of the excited electronic states and their spectroscopic parameters than previous studies. For the first time, dipole moments and their vibrationally averaged were estimated. Calculations of the effect of spin–orbit couplings on the Λ + S electronic states resulted in a dense region of states with a large number of close-lying split Ω states. Most of the states are thermodynamically stable, but for the states resulting from avoided crossings a metastability is implicit since the crossings occur at a relatively large internuclear distance and practically do not affect the characterization of the potential well. The possibility of a Coulomb explosion of the VH^{2+} molecular dication, $VH^{2+} \rightarrow V^+ + H^+$ seems to be ruled out.

Acknowledgments

J.G.F.R. acknowledges the support of Fundação de Amparo à Pesquisa do Estado de São Paulo (FAPESP, Grant # 18/14845-6) for a graduate fellowship.

Data Availability Statement

The data that support the findings of this study are available from the corresponding author upon reasonable request.

References

1. L. Pauling, "The Normal State of the Helium Molecule Ions: He_2^+ and He_2^{2+}," *Journal of Chemical Physics* 1 (1933): 56–59.

2. G. Frenking, W. Koch, D. Cremer, J. Gauss, and J. F. Liebman, "Helium Bonding in Singly and Doubly Charged First-Row Diatomic Cations HeX^{n+} (X = Li - Ne; $n = 1, 2$)," *Journal of Physical Chemistry* 93 (1989): 3397–3410.

3. R. Thissen, O. Witasse, O. Dutui, C. R. Wedlung, G. Gronoff, and J. Lilensten, "Doubly-Charged Ions in the Planetary Ionospheres: A Review," *Physical Chemistry Chemical Physics* 13 (2011): 18264–18287.

4. L. Lilensten, C. S. Wedlung, M. Barthélémy, et al., "Dications and Thermal Ions in Planetary Atmospheric Escape," *Icarus* 222 (2013): 169–187.

5. S. Falcinelli, F. Pirani, M. Alagia, et al., "Molecular Dications in Planetary Atmospheric Escape," *Atmosphere* 7 (2016): 112.

6. S. Falcinelli, F. Pirani, M. Alagia, et al., "The Escape of O^+ From the Atmosphere of Mars. An Exploration of the Observed Density Profiles on Mars," *Chemical Physics Letters* 666 (2016): 1–6.

7. S. D. Price, J. D. Fletcher, F. E. Gossan, and M. A. Parks, "Bimolecular Reactions of the Dications and Trications of Atoms and Small Molecules in the Gas Phase," *International Reviews in Physical Chemistry* 36 (2017): 145–183.

8. J. R. F. Romeu and F. R. Ornellas, "Electronic Structure, Spectroscopic Properties and Bonding in a Thermodynamically Stable Transition Metal-Containing Dication: The Case of ScS^{2+}," *Chemical Physics Letters* 754 (2020): 137706.

9. L. G. dos Santos, K. Franzreb, and F. R. Ornellas, "Thermodynamic Stability in Transition Metal- Containing Dicationic Diatomics: Examing the Case of CrO^{2+}," *Chemical Physics Letters* 771 (2021): 138525.

10. L. G. dos Santos and F. R. Ornellas, "Thermodynamic Stability of Diatomic Dications of the Families of Alkaline Earth Oxides and Hydrides: The Cases of BaO^{2+} and BaH^{2+}," *Chemical Physics* 520 (2019): 32–39.

11. L. G. dos Santos, K. Franzreb, and F. R. Ornellas, "Thermodynamically Stable Diatomic Dications: The Cases of SrO^{2+} and SrH^2," *Journal of Chemical Physics* 148 (2018): 124303.

12. G. F. de Melo and F. R. Ornellas, "The Thermodynamic Stability of Strontium Monohalides Dications: A Theoretical Exploration of the Electronic States and Spectroscopic Parameters of SrF^{2+} and $SrCl^{2+}$," *Chemical Physics Letters* 712 (2018): 118–122.

13. G. F. de Melo and F. R. Ornellas, "A High-Level Theoretical Characterization of the Electronic States and Spectroscopic Parameters of $SrBr^{2+}$ and SrI^{2+} and Thermodynamic Stability in the Family of Strontium Monohalides Dications," *Chemical Physics Letters* 722 (2019): 12–17.

14. G. F. de Melo, K. Franzreb, and F. R. Ornellas, "Exploring the Electronic States of the Hydroxil Dication OH^{2+}: Thermodynamic (Meta) stability, Bound-Free Emission Spectra, and Charge Transfer Processes," *Physical Chemistry Chemical Physics* 23 (2021): 13672–13679.

15. I. A. Lins, A. R. Belinassi, T. V. Alves, and F. R. Ornellas, "Metastability of the Low-Lying Electronic States of CBr^{2+}: A CASSC/MRCI Study," *Chemical Physics Letters* 682 (2017): 108–114.

16. A. G. S. de Oliveira-Filho and F. R. Ornellas, "The Surprising Metastability of TeH^{2+}," *Journal of Chemical Physics* 138 (2012): 224309.

17. G. F. de Melo and F. R. Ornellas, "Thermodynamic Stability and Spectroscopic Properties of Alkaline Earth Monobromides: The Cases of $MgBr^{2+}$ and $BaBr^{2+}$," *Computational & Theoretical Chemistry* 1178 (2020): 112792.

18. A. P. L. Batista, J. C. B. Lima, K. Franzreb, and F. R. Ornellas, "A Theoretical Study of SnF^{2+}, $SnCl^{2+}$, and SnO^{2+} and Their Experimental Search," *Journal of Chemical Physics* 137 (2012): 154302.

19. Y. A. Aoto, A. G. S. de Oliveira-Filho, and F. R. Ornellas, "Metastable BrO^{2+} and NBr^{2+} in the Gas Phase," *Journal of Chemical Physics* 134 (2011): 104303.

20. K. L. Kunze and J. F. Harrison, "Electronic Structure of the Thermodynamically Stable ScN^{2+} Dication," *Journal of Physical Chemistry* 95 (1991): 6418–6420.

21. S. Petrie, "ScF^{2+} and $ScHe^{3+}$: Two Highly-Charged Episodes of the Gas Phase Adventures of Scandium," *Chemical Physics Letters* 399 (2004): 475–479.

22. H. F. Harrison and K. L. Kunze, "The Electronic Structure of the Neutral, Mono- and Dipositive Transition Metal Nitrides, ScN, TiN, VN, CrN," in *Organometallic Ion Chemistry. Understanding Chemical Reactivity*, vol. 15, ed. B. S. Freiser (Dordrecht: Springer, 1996), 89–122.

23. J. F. Harrison and P. S. Christopher, "Electronic Structure of the Dipositive Transition Metal Hydrides ScH^{2+}, TiH^{2+}, VH^{2+}, CrH^{2+} and MnH^{2+}," *Molecular Physics* 96 (1999): 31–42.

24. D. J. D. Wilson, C. J. Mardsen, and E. I. V. Nagy-Felsobuki, "Ab Initio Structures and Stabilities of Doubly Charged Diatomic Metal Hydrides for the First Row Transition Metals," *Journal of Physical Chemistry A* 106 (2002): 7348–7354.

25. D. J. D. Wilson, C. J. Mardsen, and E. I. V. Nagy-Felsobuki, "Ab Initio Structures and Stabilities of $HeTM^{3+}$ (TM=Sc-Cu)," *Chemical Physics* 284 (2002): 555–563.

26. D. J. D. Wilson, C. J. Mardsen, and I. E. V. Nagy-Felsobuki, "Ab Initio Calculations on First Row Transition Metal Hydrides TMH^{n+} and Helides $TMHe^{(n+1)+}$ (TM=Sc-Cu, n=0-2)," *Physical Chemistry Chemical Physics* 5 (2003): 252–258.

27. J. Klos, M. F. Rode, J. E. Rode, G. Chalasinski, and M. M. Szczesniak, "Interactions of Transition Metal Atoms With He," *European Physical Journal D: Atomic, Molecular, Optical and Plasma Physics* 31 (2004): 429–437.

28. J. F. Harrison, "Electronic Structure of Diatomic Molecules Composed of a First-Row Transition Metal and Main-Group Element (H-F)," *Chemical Reviews* 100 (2000): 679–716.

29. J. G. F. Romeu and F. R. Ornellas, "Electronic States, Spectroscopic Properties, Electronic Transitions, and Bonding in ScH^{2+}: A Thermodynamic Stable Transition Metal-Hydrogen Dication," *Journal of Quantitative Spectroscopy and Radiative Transfer* 310 (2023): 108747.

30. B. O. Roos, P. R. Taylor, and P. E. M. Siegbahn, "A Complete Active Space SCF (CASSCF) Using a Density Matrix Formulated Super-CI Approach," *Chemical Physics* 48 (1980): 157–173.

31. P. J. Knowles and H.-J. Werner, "A Second Order Multiconfiguration SCF Procedure With Optimum Convergence," *Journal of Chemical Physics* 82 (1985): 5053–5063.

32. H.-J. Werner and P. J. Knowles, "An Efficient Second Order MCSCF Method for Long Configuration Expansions," *Chemical Physics Letters* 115 (1985): 259–267.

33. P. J. Knowles and H.-J. Werner, "An Efficient Method for the Evaluation of Coupling Coefficients in Configuration Interaction Calculations," *Chemical Physics Letters* 145 (1988): 514–522.

34. H.-J. Werner and P. J. Knowles, "An Efficient Internally Contracted Multiconfiguration–Reference Configuration Interaction Method," *Journal of Chemical Physics* 89 (1988): 5803–5814.

35. E. R. Davidson and D. W. Silver, "Size Consistency in the Dilute Helium Gas Electronic Structure," *Chemical Physics Letters* 52 (1997): 403–406.

36. H.-J. Werner, M. Kállay, and J. Gauss, "The Barrier Height of the F + H_2 Reaction Revisited: Coupled-Cluster and Multireference Configuration-Interaction Benchmark Calculations," *Journal of Chemical Physics* 128 (2008): 034305.

37. "MOLPRO Is a Package of Ab Initio Programs," written by H.-J. Werner,P. J. Knowles, with contributions of J. Almlöf, D. Amos, A. Berning, et al.

38. N. B. Balabanov and K. A. Peterson, "Systematically Convergent Basis Sets for Transition Metals. I. All-electron Correlation Consistent Basis Sets for the 3d Elements Sc–Zn," *Journal of Chemical Physics* 123 (2005): 064107.

39. T. H. Dunning, Jr., "Gaussian Basis Sets for Use in Correlated Calculations. I. The Atoms Boron Through neon and Hydrogen," *Journal of Chemical Physics* 90 (1989): 1007–1023.

40. G. Herzberg, *Molecular Structure and Molecular Spectra I: Spectra of Diatomic Molecules*, 2nd ed. (New York: Van Nostrand Reinhold, 1950), 315.

41. A. Kramida, R. Yu, J. Reader, and NIST ASD Team, *NIST Atomic Spectra Database* (Gaithersburg, MD: National Institute of Standards and Technology, see 5.6.1, 2018), https://doi.org/10.18434/T4W30F.

42. W. T. Zemke and W. C. Stwalley, "INTENSITY: Transition Probabilities for Diatomic Molecules," *QCPE Bulletin* 4 (1981): 79.

43. F. R. Ornellas, F. B. C. Machado, and O. Roberto-Neto, "A Theoretical Study of the Molecules BeF and BeF^+ in Their Lowest-Lying Electronic States," *Molecular Physics* 77 (1992): 1169–1185.

44. F. R. Ornellas, O. Roberto-Neto, A. C. Borin, and F. B. C. Machado, "On the Low-Lying Electronic States of the Molecule BeN," *Journal of Chemical Physics* 95 (1991): 9086–9093.

45. F. R. Ornellas and S. Iwata, "A Theoretical Study of the Electronic Structure and Spectroscopic Properties of the Low-Lying Electronic States of the Molecule SiB," *Journal of Chemical Physics* 107 (1997): 6782–6794.

46. A. Berning, M. Schweizer, H. J. Werner, P. J. Knowles, and P. Palmieri, "Spin-Orbit Matrix Elements for Internally Contracted Multireference Configuration Interaction Wavefunctions," *Molecular Physics* 98 (2000): 1823–1833.

47. G. Knizia, "Intrinsic Atomic Orbitals: An Unbiased Bridge Between Quantum Theory and Chemical Concepts," *Journal of Chemical Theory and Computation* 9 (2013): 4834–4843.

48. J. G. F. Romeu, G. F. de Melo, and F. R. Ornellas, "Characterizing Electronic States and Spectra in Transition Metal-Rare Gas Diatomic Cations: The Cases of VAr^+ and VKr^+," *Journal of Quantitative Spectroscopy and Radiative Transfer* 277 (2022): 107959.

49. C. W. Bauschlicher, Jr., "Large Atomic Natural Orbital Basis Sets for the First Transition Row Atoms," *Theoretica Chimica Acta* 92 (1995): 183–198.

50. H. J. Partridge, "Near Hartree-Fock Quality GTO Basis Sets for the 1st and 3rd Row Atoms," *Journal of Chemical Physics* 90 (1989): 1043–1047.

51. R. A. Kendall, T. H. Dunning, Jr., and R. J. Harrison, "Electron Affinities for the 1st Row Atoms Revisited – Systematic Basis Sets and Wavefunctions," *Journal of Chemical Physics* 96 (1992): 6796–6806.

52. W. G. Richards, J. Raftery, and R. K. Hinkley, *Theoretical Chemistry, Vol. 2*, R. N. Dixon (London: Chemical Society, 1973) (Chapter 12).

Supporting Information

Additional supporting information can be found online in the Supporting Information section.